Compared abilities of filled and unfilled natural rubbers to crystallize in a large strain rate domain

Nicolas Candau [a,b], *Laurent Chazeau* *[,a,b], *Jean-Marc Chenal* [a,b], *Catherine Gauthier* [c], *Etienne Munch* [c]

[a]Université de Lyon, CNRS, France

[b]MATEIS, INSA-Lyon, CNRS UMR5510, F-69621, France

[c] Michelin, Centre de technologies, 63040 Clermont Ferrand Cedex 9, France

*Corresponding author: Tel: +33472438357, E-mail address: laurent.chazeau@insa-lyon.fr (L. Chazeau)

Abstract

Strain induced crystallization (SIC) in filled and unfilled natural rubbers is investigated through in situ wide angle X-rays scattering (WAXS) experiments at various strain rates. The values of local stretching ratio at SIC onset ($\lambda_{c,local}$) are found similar between filled and unfilled rubbers stretched at slow strain rate (10^{-3} s^{-1}) and in a large temperature range [21°C, 80°C]. This is consistent with the fact that the calculated 'local' network densities of the first chains involved in SIC are very close in all samples. Conversely, $\lambda_{m,local}$ for tests carried out in a large temperature range [21°C,80°C] is found higher in filled samples compared to unfilled one due to a lower crystallites size. In order to investigate SIC in filled and unfilled rubbers submitted to conditions of solicitations met in pneumatic tires, in situ WAXS experiments are performed during high strain rates cycles (10-100 s^{-1}) thanks to

a recent homemade machine. By increasing the frequency, strong self-heating related to filler-rubber interaction causes a dramatic fall of the crystallinity index (CI) in filled rubber.

Keywords: Strain induced crystallization, A. Polymer-matrix composites (PMCs), D. X-rays diffraction (XRD)

1. Introduction

Carbon black filler is an essential component in pneumatic industry. It strongly improves mechanical properties, tensile strength, wear and abrasion resistance of rubbers. Because fillers are undeformable particles, when a filled rubber sample is stretched at a given macroscopic stretching ratio λ, the extension of the rubbery matrix (λ_{local}) is amplified. This increases the stress, as proved experimentally [1-3] and demonstrated by mechanical model [4]. Such a strain amplification leads to a decrease of the stretching ratio at SIC onset (λ_c) and of the melting stretching ratio (λ_m) measured at room temperature [1-3, 5], while the crystallization temperature T_c and the melting temperature T_m at fixed λ are increased [2, 5]. The presence of fillers is also known to strongly impede the crystallite growth [1,3,5]. In spite of this, the crystallite size is rarely considered when the abilities of unfilled and filled rubbers to crystallize under strain are compared. In addition, most of the studies of the literature are performed at slow strain rate (around 10^{-3} s^{-1}), i.e. far from the loading conditions of rubber in pneumatic tires (10–100 s^{-1}). Only the recent paper of Brüning [6] shows that, for a given macroscopic stretching ratio (i.e. without taking into account any strain amplification), SIC characteristic time is lowered in presence of fillers.

In this paper, we first propose a complete thermodynamic description of SIC in filled

and unfilled rubbers by considering simultaneously the local stretching ratio, the local density of the chains involved in SIC and the crystallite sizes. These parameters are estimated from in situ WAXS. A comparative study of SIC in filled and unfilled rubbers during dynamic cycles at high strain rates is then performed thanks to a new homemade machine. The results are discussed within the frame of the previously developed model.

2. Materials

The materials of the study are one crosslinked unfilled natural rubber (NR) and two filled natural rubbers obtained by sulphur vulcanization of gum. The material recipe is the following: rubber gum (100 phr) which is a Technically Specified Rubber (TSR20) provided by Michelin Tire Company, stearic acid (2 phr), ZnO (1.5 phr), 6PPD (3 phr), CBS (1.9 phr) and sulfur (1.2 phr) (where phr means g per 100 g of rubber). In addition, the two-studied carbon black filled materials contain 20 and 50 phr of fillers (F_{20}NR and F_{50}NR). Dumbbell-shaped samples, with a 6mm gauge length (l_0) and 0.8 mm thickness, are machined. The average network chain density (ν) is estimated from the swelling ratio (Q_{pol}) in toluene and from the Flory–Rehner equation [7]. Q_{pol} is found equal to 5.17, 4.57 and 4.12 for NR, F_{20}NR and F_{50}NR samples respectively. Within the assumption of a perfect interface, the relation between the swelling ratio of the polymer itself (Q_{pol}) and the swelling ratio of the composite is deduced from the Kraus equation [4]. This allows estimating the density of an 'effective' network chain ν_{eff} (sum of chemical crosslinks, trapped entanglements and nodes made of elastomer chains adsorbed on the filler surface), which value is equal to 1.42, 2.09 and 2.9 ($\times 10^{-4}$ mol.cm^{-3}) for NR, F_{20}NR and F_{50}NR samples respectively.

3. In situ WAXS during slow strain rate and dynamic cycles

The in situ WAXS measurements during slow strain rate cycles are carried out on the D2AM beamline of the European Synchrotron Radiation Facility (ESRF). The two-dimensional (2D) WAXS patterns are recorded by a CCD Camera (Princeton Instrument). The procedure to analyze the scattering pattern is extensively described in a previous paper [8]. The crystallinity index CI is then determined as follows [9]:

$$CI = \frac{I_{a0} - I_{a\lambda}}{I_{a0}} \tag{1}$$

where I_{a0} and $I_{a\lambda}$ are the intensities of the amorphous phase at the peak top in the unstretched state and the stretched state, respectively. The average crystallite sizes L_{hkl} (L_{200}, L_{102} and L_{002}) are estimated from the Scherrer equation:

$$L_{hkl} = \frac{K\lambda_w}{\beta_{1/2} cos\theta} \tag{2}$$

where λ_w (1.54 Å) is the wavelength and θ is the Bragg angle. In this study, each crystalline peak is fitted with a Lorentzian function in which the width at half-height is $\beta_{1/2}$ and K value is 0.64 [1, 10]. In filled and unfilled samples $L_{002} = c_1$ is found independent of the mechanical loading [8] or temperature of the test [11]. An empiric relationship between the lateral sizes of crystallites has been established: $b_1 \sim a_1/3$ with $L_{200} = a_1$ and $L_{020} = b_1$. It must be noted that such relationship has already been found in many other studies [3, 6, 10]. The b_1 value is deduced from the measurement of L_{120}. Given the assumption of a parallepedic shape for the crystallites, b_1 (L_{020}) is equal to $0.94L_{120}$. The average volume of the crystallites is then defined by $V = 0.94L_{120}L_{200}L_{002}$.

The in situ WAXS measurements during dynamic cycles are carried out on the Diffabs beamline of the French national Synchrotron SOLEIL. These tests are performed with a dedicated new apparatus [12]. They consist in rapidly pre-stretching the sample at λ_a and maintaining the deformed state during five minutes; then dynamically deforming the sample around λ_a from 2 Hz to 80 Hz with the amplitude $\Delta\lambda = \lambda_{max} - \lambda_{min}$. Self-heating is estimated thanks to the measurement of the sample surface temperature with an Infra-Red pyrometer (CTLF-CF3-C3, Microepsilon). In order to record a proper mechanical response, the experiments are repeated in exactly same conditions on another dynamic machine. For all the tests, the nominal stretching ratio λ is accurately measured by video extensometer. In order to avoid an uncontrolled Mullins effect during the different tests, all the samples were stretched four times above the maximum stretching ratio expected during the tests.

4. Results and discussion

4.1. Thermal stability of strain induced crystallites

Figure 1 shows the CI and crystallite size of filled and unfilled NR samples stretched cyclically at room temperature (21°C) and slow strain rate ($4.2 \times 10^{-3}\ s^{-1}$). CI increases and decreases during loading and unloading respectively, as shown in figure 1a. The hysteretic shape is classically explained by the kinetics of the crystallization process: an energy barrier must be crossed in order to allow crystallites nucleation, whereas melting is instantaneous at this strain rate. The CI curves are shifted to lower λ when the filler content increases, as already shown in previous papers [1-3, 5]. More specifically, the stretching ratio at the SIC onset (λ_c) and the melting stretching ratio (λ_m) are decreased. This is commonly explained in literature by a strain amplification in the rubbery matrix due to the

presence of fillers, which act as non-deformable particles. The increase of crystallite size with strain is consistent with references [1, 8, 10, 11] but not with references [3, 5, 13]. In a previous work, we stated that such discrepancy should be due to the different methodologies of WAXS analysis used by the authors [8]. Anyhow, all studies report a limitation of the crystallite size in presence of fillers [1, 3, 5], as evidenced in figure 1b.

To characterize the effect of the stretching ratio on the melting (figure 2), samples are now stretched up to different λ values at 21°C and slow strain rate, relaxed during five minutes (in order to stabilize the crystalline phase) and then submitted to a heating ramp (around 2K/min). The relation between CI and L_{200} is the same as the one found during unloading at 21°C (unpresented data). As expected, the melting temperature T_m increases with λ (cf. The two curves of the F_{20}NR samples). In spite of a higher λ and also a larger crystallite size, T_m in the unfilled sample stretched at $\lambda = 6$ is lower than the one in F_{20}NR sample stretched at $\lambda = 4.4$. This suggests that T_m is mainly controlled by strain amplification induced by presence of fillers. In literature, the strain amplification factor (A) is defined as the ratio of the local strain $\varepsilon_{local} = \lambda_{local} - 1$ for a filled rubber over its macroscopic strain $\varepsilon = \lambda - 1$. Several models allow predicting its evolution as a function of the filler volume fraction φ [14, 15]. For an homogeneous matrix filled with polydisperse rigid spheres, A can be deduced from the Nielsen formula [15]:

$$A = \frac{1}{1 - \varphi^{1/3}} \tag{3}$$

where the 1/3 factor refer to a system with a 3-dimensional arrangement of monodisperse spherical particles. The effect of the fillers on λ_m is rather difficult to estimate because it

depends on both amplification factor and crystallite size. Conversely, the appearance of the first crystallites at λ_c during loading might be only governed by the local extension of the molecules. With this assumption, the experimental amplification factor A_e can be deduced from the ratio λ_c *(NR)*/λ_c (F-NR). A_e values found for F_{20}NR and F_{50}NR samples and extracted from experiments performed on filled and unfilled NR during stretching at 21°C and slow strain rate (~ 10^{-3} s^{-1}), are plotted on figure 3 [1,16,17]. They are well fitted by equation (3), especially the data of our study (note that they are largely underestimated by the hydrodynamic factor $A = 1 + 2.5\varphi + 14\varphi^2$ [14]). These results strongly support the idea that $\lambda_{c,local}$ is the same with or without fillers. It is consistent with the reported fact that λ_c is the same for vulcanized rubbers with different crosslink densities [10, 13]. With the Nielsen correction applied to the melting process, $\lambda_{m,local}$ at 21°C is found equal to 3.8 and 3.5 for F_{50}NR and F_{20}NR respectively, whereas it is 3 in unfilled sample. Thus, $\lambda_{m,local}$ at 21°C is found lower in unfilled sample. At this stage, this can be explained by the larger size of the NR crystallites measured at λ_m (figure 1b).

The classical theory of phase transition [18] can be used to interpret the combined effect of crystallite size and stretching ratio on melting temperature (i.e. on thermal stability of crystallites). The crystallites are assumed to grow spontaneously – compared to the time scale of the experiment – up to their saturation size in all the directions ($a_{sat} = a_1$ and $b_{sat} = b_1 \sim a_1/3$ [8] and c_{sat}). An estimate of the average number of crystallites N = CI/V during loading at 21°C, shows that crystallization is the result of successive appearance of crystallites [8]. The melting is the result of successive disappearance of crystallites in the inverse order. Thus, the crystallite size measured at λ close to λ_m corresponds to the one of

the most stable crystallites. These crystallites are also the first to appear at λ_c. Assuming then an affine deformation of chains, the melting temperature can be estimated as a function of the stretching ratio and the crystallite size [11]:

$$T_m = \frac{T_{m,\infty}\left(1 - \frac{1}{\Delta H_m}\left(\frac{8\sigma_l}{a_{sat}} + \frac{2\sigma_e}{c_{sat}}\right)\right)}{1 - \frac{\nu_{local}\, RT_{m,\infty}}{2\Delta H_m}\left({\lambda_{m,local}}^2 + \frac{2}{\lambda_{m,local}} - 3\right)} \quad (4)$$

where ΔH_m is the melting enthalpy ($\Delta H_m = 6{,}1 \times 10^7$ J.m^{-3} [19]), $T_{m,\infty}$ is the melting temperature of the infinite crystal in the undeformed state ($T_{m,\infty} = 35.5°$ [20]), R is the constant of the perfect gazes ($R = 8.314$ J.mol^{-1}.K^{-1}). σ_e and σ_l are the chain end energy and lateral surface energies respectively ($\sigma_e = 0.66 \times 10^{-2}$ Jm^{-2} and $\sigma_l = 0.33 \times 10^{-2}$ Jm^{-2} calculated in ref. [8]). $c_{sat} = c_1 = L_{002}$ is found independent of the stretching ratio or temperature of the test, but decreases in presence of fillers (85 Å, 77 Å and 55 Å for NR, F_{20}NR and F_{50}NR respectively). a_{sat} (L_{200}), corresponding to the incipient crystalline structure (estimated for CI = 0.5%) is equal to 50 Å, 45 Å and 40 Å for NR, F_{20}NR and F_{50}NR respectively (figure 1b). Assuming heterogeneities of the material, ν_{local} is not the average value of the network density (ν_{eff}) but the network density of the last crystallites that melt. From equation (4) taken at 21°C and at $\lambda_{m,local}$, ν_{local} is found around 4×10^{-4} mol.cm^{-3} (+/- 0.1×10^{-4} mol.cm^{-3}) for all samples. Recalling that these crystallites are the ones which crystallize at $\lambda_{c,local}$, this result is consistent with the initial assumption of a similar local stretching ratio between filled and unfilled samples. From the knowledge of ν_{local} and the size of the most stable crystallites, theoretical T_m are plotted in figure 4 as a function of λ and λ_{local}. The fits are compared to experimental values extracted from the above tests. Our experimental data set

for NR is completed thanks to an experiment consisting in heating a stretched sample at λ_m = 5.3 up to T_m (found equal to 80°C). Fits are found in good agreement with experimental data. They confirm that, for a given local stretching ratio, T_m in filled rubber is lower due to the smaller size of crystallites. Only one experimental couple of values (λ_{local} = 7.1, T_m = 120°C) does not coincide with the prediction from equation 4 (λ_{local} = 7.1, T_m = 174°C). This can be explained by the degradation of the network chains involved in SIC, which can occur at high temperature and can be eased at high stretching ratio [21]. To check this scenario, the sample of the concerned test was re-crystallized during cooling at same stretching ratio. Re-crystallization was initiated at T_c = 110°C which is logically lower than T_m = 120°C, due to supercooling. However, CI at the end of the cooling (i.e. at 21°C) should have been similar to the CI measured at 21°C just before heating, i.e. 10% (figure 2). Actually, the CI value measured at 21°C was only 5.7%, supporting the above assumption of a degradation of the chains.

4.2. Effect of the temperature on SIC during stretching at slow strain rate

Samples are now stretched at slow strain rate (4.2×10^{-3} s^{-1}) and different temperatures (21°C, 50°C and 80°C). Due to a limitation of the maximum stretching ratio allowed by the experimental device, λ_c for NR stretched at 80°C was estimated from the mechanical response following the method presented in ref. [22] and found around 5.9. For all samples, when the temperature increases, λ_c increases and the slope dCI/dλ slightly decreases, which is consistent with the literature [2]. As discussed previously, $\lambda_{c,local}$ value measured at 21°C does not depend on the filler content (figure 5b). For higher temperatures, similar $\lambda_{c,local}$ values are also obtained. This strongly supports our previous analysis. The slope dCI/dλ_{local}

at 21°C decreases with the quantity of fillers. This was also observed in ref. [1] in which same correction factor was applied. This is likely explained by a limitation of the crystallite growth in presence of fillers (cf. figure 1b). Same trend is observed at 50°C but not at 80°C. This suggests that the strain amplification factor is not sufficient to understand the effect of the fillers on the CI(λ_{local}) at high temperature, one SIC has begun.

Crystallization occurs when the energy barrier of nucleation $\Delta\varphi^*$ is low enough to allow the formation of a stable nucleus. This is done by increasing λ or decreasing T. It can be proposed that a temperature increase (which would lead to an increase of the energy barrier) must be compensated by an increase of the stretching ratio in order to allow nucleation in the range of the experimental time. Within this assumption, the energy barrier $\Delta\varphi^*$ is thus found independent of the temperature of the test (its literal expression can be found in ref. [8]) and T_c can be written [11]:

$$T_c = \frac{T_{m,\infty}\left(1 - \frac{1}{\Delta H_m}\sqrt{\frac{32{\sigma_l}^2\sigma_e}{\Delta\varphi^*}}\right)}{1 - \frac{\nu_{local}\,RT_{m,\infty}}{2\Delta H_m}\left({\lambda_{c,local}}^2 + \frac{2}{\lambda_{c,local}} - 3\right)} \tag{5}$$

For each sample, $\Delta\varphi^*$ is calculated from equation (5) at 21°C and $\lambda_{c,local}$. T_c can then be estimated as a function of λ and λ_{local} (figure 6). Recalling that ν_{local} is found similar for all samples and that the $\lambda_{c,local}$ values are very close at 21°C, equation (5) predicts that, for a given local stretching ratio, T_c does not depend on the quantity of fillers. For sake of comparison, the data (λ_c, T_c) and (λ_{clocal}, T_c) extracted from the above experiments (figure 5) are added. Predictions from equation (5) is satisfactory at stretching ratio and temperature

low enough to avoid any degradation of the network chains involved in SIC. Indeed, due to this degradation, T_c measured for filled sample at $\lambda_{local} = 7.1$ and re-crystallized by cooling is found equal to 110°C, which is much lower than the predicted value ($T_c = 146$°C).

4.3. SIC during dynamic cycles at high frequency

NR and F_{50}NR samples are now dynamically stretched at high frequency thanks to a new experimental device (see section 3) in order to mimic the conditions of solicitation of rubber in pneumatic tire. Samples are first pre-stretched at λ_a and dynamically deformed around λ_a with an amplitude $\Delta\lambda = \lambda_{max} - \lambda_{min} = 1.8$ for the unfilled samples. λ_a and $\Delta\lambda$ in filled samples are chosen in order to have the same local stretching amplitudes (calculated with the Nielsen correction). For the first series (figure 7a), λ_a is low enough to have $\lambda_{min} \leq \lambda_m$ at 21°C. For the second series, $\lambda_{min} > \lambda_m$ at 21°C (figure 7b).

For the first series, because $\lambda_{min} \leq \lambda_m$ at 21°C, CI at λ_{min} (CI_m) is equal to zero. CI at λ_{max} (CI_M) is plotted on figure 8 as a function of the stretching time (half-time of the cycle). CI values reached at $\lambda = \lambda_{max}$ during the unloading step of the cyclic test at slow strain rate are added (figure 1). These values are assumed to correspond to the equilibrium state. From the equilibrium state to dynamic conditions, the CI_M values in both samples strongly decrease due to strain rate and self-heating effects, and reach very similar values for the shortest experimental times. The concomitant effects of self-heating and strain rate are more deeply discussed for the second series of test.

Figure 9a presents the evolution of self-heating (estimated by the difference ΔT between surface temperature of the sample and 21°C) versus the stretching time for the second series of test. Self-heating strongly increases with frequency due to viscoelastic dissipation;

this effect is more important in filled sample due to friction at the interface between the rubbery matrix and the carbon black particles. Assuming that a crystalline cycle is associated with a certain number of crystallites which nucleate and instantaneously grow during loading, and totally melt during unloading, CI at λ_{min} (CI_m) should be the result of other crystallites that are not involved in the dynamic cycle [8]. Thus, CI_m should not decrease if the temperature is maintained constant. This is confirmed on figure 9b, showing that the CI is unchanged between the equilibrium state and 2 Hz (250msec), i.e. when self-heating is negligible. Then, by increasing the frequency, CI_m strongly decreases and disappears at 10-20 Hz (25-50msec) and 5-10 Hz (50-100msec) in unfilled and filled NR respectively. At these frequencies, the temperature at the sample surface becomes high enough to justify a shift of the λ_m values up to λ_{min} (cf. figure 4), i.e. a disappearance of CI_m.

Variations of CI involved in dynamic cycles, $\Delta CI = CI_M - CI_m$, also decrease with frequency (figure 10), probably due to combined effects of strain rate and self-heating. For the lowest frequencies (like for the cyclic test at slow strain rate), ΔCI is found higher in the unfilled NR sample, which is probably explained by its higher ability to form large crystallites but also to a lower self-heating. The ΔCI values then converge for a critical frequencies around 10 Hz-20 Hz (25-50 msec). This is expected, because these frequencies are high enough to suppress the crystallinity at λ_{min}; and the conditions become similar to the one met with the first series of test, i.e. $\lambda_{min} \leq \lambda_m$ at the sample temperature. For the highest frequencies (above 20 Hz), self-heating becomes so important in filled sample that its CI fall below the CI measured in unfilled sample.

The evolution of CI and of the mechanical response during the whole cycle is now

presented for two frequencies 2 Hz and 10 Hz (figures 11 a-d). Both crystalline and mechanical cycles present hysteresis (figures 11 a-b and 11 c-d respectively). Obviously, the CI decrease with frequency previously observed at λ_{min} and λ_{max} is also observed for all the positions of the cycle (figures 11 a-b). To suppress the entropic effect caused by self-heating (figure 9a), in figure 11c and 11d, stress is corrected from the ratio 294/ (294 + ΔT). Concerning this mechanical response, two trends are reported depending on the presence of fillers. In unfilled rubber (figure 11c), when frequency increases, the stress increases (decreases) for stretching ratios below (above) λ_a. This means that the well-known relaxation and hardening effects typical for SIC at slow strain rate [22] are progressively hindered at high strain rates. For filled rubber, the increase of the frequency is associated with a strong decrease of the stress, especially at the highest stretching ratio (figure 11d). Thus, the strong hardening effect, usually mentioned for tests performed at much lower strain rate (commonly explained by the creation of a 'giant network' [2] made of strain induced crystallites and fillers) tends to disappear in such drastic conditions of solicitation.

5. Conclusion

Strain induced crystallization was studied in filled and unfilled natural rubbers during in situ WAXS experiments performed at slow strain rate (~10^{-3} s^{-1}) and high strain rates (10-100 s^{-1}). The results were analysed with a thermodynamic description taking into account the crystallite sizes, the local stretching ratio and the "local" network chains density. The local stretching ratio at SIC onset calculated with the appropriate strain amplification factor is found independent of the presence of fillers in a large range of temperature [21°C, 80°C] and at slow strain rate. From this approach, we found that (i) the chains involved in the first

crystallites have similar local density and that (ii) for a given local stretching ratio, the melting temperature is lower in filled sample, due to smaller crystallites.

SIC in filled and unfilled rubber is then investigated at high strain rates thanks to a new homemade machine. For a given local stretching ratio and low frequency, the CI in filled rubber is still found lower than in unfilled one, and again explained by smaller crystallites. The CI value then rapidly decreases by increasing the frequency due to the combined effect of strain rate and self-heating. For the highest strain rates, self-heating generated by the friction at the filler/matrix interface becomes strong enough to cause the earlier disappearance of CI in filled rubber compared to unfilled one.

5. Acknowledgements

The authors are indebted to the European Synchrotron Radiation Facility (ESRF) and Dr. C. Rochas, on the one hand and to the synchrotron SOLEIL and D. Thiaudière on the other hand for providing the necessary beamline time and technical assistance in the experiments on the D2AM line and DiffAbs line respectively.

6. References

[1] J. M. Chenal, C. Gauthier, L. Chazeau, L. Guy and Y. Bomal. Parameters governing strain induced crystallization in filled natural rubber. Polymer 2007; 48 (23): 6893-6901.

[2] J. Rault, J. Marchal, P. Judeinstein and P. A. Albouy. Stress-induced crystallization and reinforcement in filled natural rubbers: 2H NMR study. Macromolecules 2006; 39 (24): 8356-8368.

[3] S. Trabelsi, P.A. Albouy, and J. Rault. Effective local deformation in stretched filled rubber. Macromolecules 2003; 36 (24): 9093-9099.

[4] G. Kraus. Reinforcement of elastomers by carbon black. Rubber Chem. Technol 1978; 51 (2): 297-321.

[5] S. Poompradub, M. Tosaka, S. Kohjiya, Y. Ikeda, S. Toki, I. Sics and B. S. Hsiao. Mechanism of strain-induced crystallization in filled and unfilled natural rubber vulcanizates. J. Appl. Phys 2005; 97 (10): 103529-1-103529-9.

[6] K. Bruning, K. Schneider, S. V. Roth and G. Heinrich. Kinetics of Strain-induced crystallization in natural rubber studied by WAXD: Dynamic and impact tensile experiments. Macromolecules 2012; 45 (19): 7914-7919.

[7] P. J. Flory and J. Rehner. Statistical mechanics of cross-linked polymer networks II. Swelling. J. Chem. Phys 1943; 11 (11): 521-526.

[8] N. Candau, R. Laghmach, L. Chazeau, J-M. Chenal, C. Gauthier, T. Biben and E. Munch. Strain-Induced Crystallization of Natural Rubber and Cross-Link Densities Heterogeneities. Macromolecules 2014; 47 (16): 5815-5824.

[9] G. R. Mitchell. A wide-angle X-ray study of the development of molecular orientation in crosslinked natural rubber. Polymer 1984; 25 (11): 1562-1572.

[10] J. M. Chenal, L. Chazeau, L. Guy, Y. Bomal and C. Gauthier. Molecular weight between physical entanglements in natural rubber: A critical parameter during strain-induced crystallization. Polymer 2007; 48 (4): 1042-1046.

[11] N. Candau, L. Chazeau, J-M. Chenal, C. Gauthier, R. Laghmach, T. Biben and E. Munch. Temperature dependence of strain-induced crystallization in natural rubber:

on the presence of different crystallite populations. Submitted to Polymer.

[12] N. Candau, L. Chazeau, J. M. Chenal, C. Gauthier, J. Ferreira, E. Munch and C. Rochas. Characteristic time of strain induced crystallization of crosslinked natural rubber. Polymer 2012; 53 (13): 2540-2543.

[13] M. Tosaka, S. Murakami, S. Poompradub, S. Kohjiya, Y. Ikeda, S. Toki, I. Sics and B. S. Hsiao. Orientation and crystallization of natural rubber network as revealed by WAXD using synchrotron radiation. Macromolecules 2004; 37 (9): 3299-3309.

[14] E. Guth and O. Gold. On the hydrodynamical theory of the viscosity of suspensions. Physical Review 1938; 53 (322): 2-15.

[15] L.E. Nielsen. Simple theory of stress-strain properties of filled polymers. Journal of Applied Polymer Science 1966; 10 (1): 97-103.

[16] J. Marchal. Cristallisation des caoutchoucs chargés et non chargés sous contrainte: effet sur les chaînes amorphes. Ph.D. Thesis 2006; Université Paris Sud-Paris XI.

[17] S. Dupres. Dynamique, déformations locales et irréversibilités dans des élastomères renforcés par du noir de carbone. Ph.D. Thesis 2006; Université Paris Sud-Paris XI.

[18] L. H. Sperling, Introduction to physical polymer science 2005 (Wiley.com).

[19] H. G. Kim and L. Mandelkern. Multiple melting transitions in natural rubber. Journal of Polymer Science Part A-2: Polymer Physics 1972; 10 (6): 1125-1133.

[20] E. N. Dalal, K. D. Taylor and P. J. Phillips. The equilibrium melting temperature of cis-polyisoprene. Polymer 1983; 24 (12): 1623-1630.

[21] R. Fraser, T. Macrae, A. Miller and R. D. Rowlands. Digital processing of fibre diffraction patterns. Journal of Applied Crystallography 1976; 9 (2): 81-94.

[22] Y. Miyamoto, H. Yamao and K. Sekimoto. Crystallization and melting of polyisoprene rubber under uniaxial deformation. Macromolecules 2003; 36 (17): 6462-6471.

Figure Captions

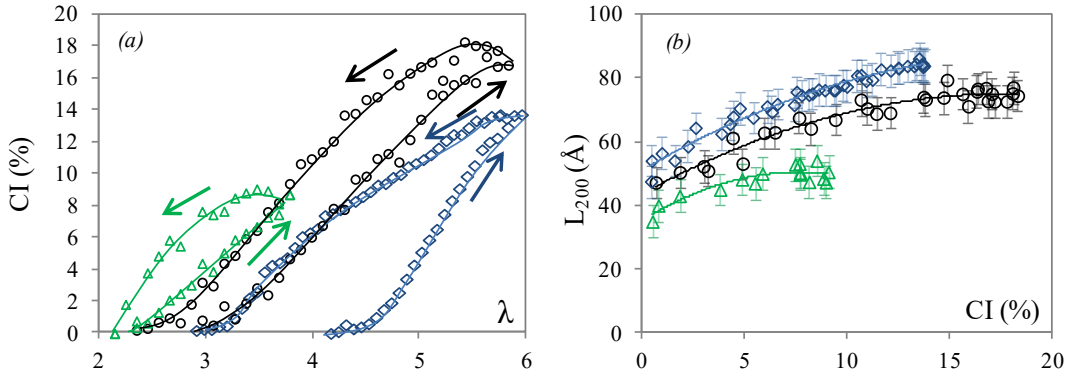

Figure 1. (a) CI during cyclic test at 21°C and slow strain rate (4.2×10^{-3} s^{-1}) for NR (diamond symbols), F_{20}NR (circle symbols) and F_{50}NR (triangle symbols). Arrows indicate the direction of the cycles. (b) L_{200} versus CI during the unloading.

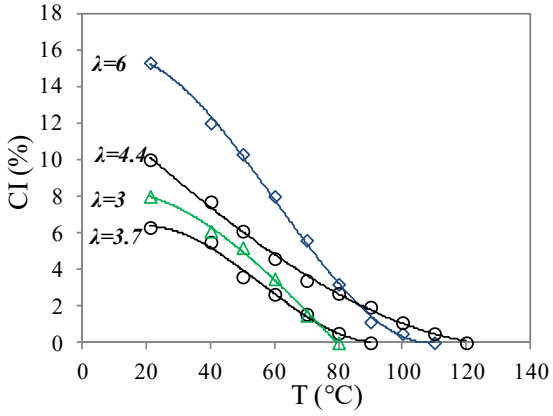

Figure 2. CI versus temperature during heating in the deformed state for NR stretched at λ

= 6 (diamond symbols), F_{20}NR stretched at λ = 3.7 and λ = 4.4 (circle symbols), and F_{50}NR stretched at λ = 3 (triangle symbol).

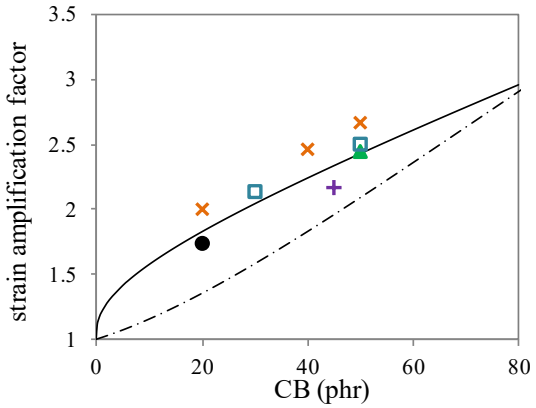

Figure 3. A_e values from experiments performed at 21°C and slow strain rates as a function of the fraction of fillers (in phr). Values are extracted from the present study (filled circle and filled triangle) and from ref. [1] (plus), ref. [16] (cross), ref. [17] (square). Theoretical trends of A estimated from the Nielsen formula (solid line) and from the hydrodynamic relation (dash dotted line) are added.

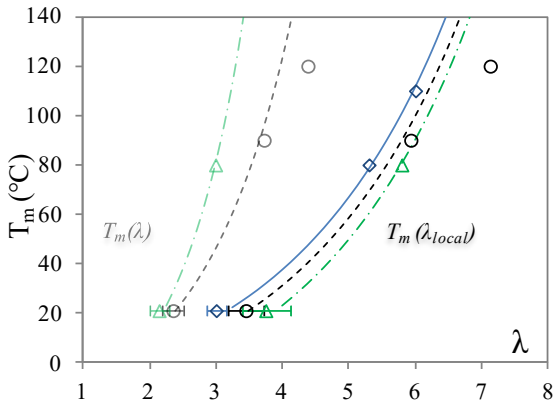

Figure 4. T_m versus λ and λ_{local} for NR (diamond symbols), F_{20}NR (circle symbols), F_{50}NR

(triangle symbols). Lines are prediction of T_m from equation (4) and for NR (solid line), F_{20}NR (dotted line) and F_{50}NR (dashed-dotted line). The error bar is equal to +/-0.15 for λ_m at 21°C and +/-0.15*A* for $\lambda_{m,local}$ at 21°C (with *A* extracted from the Nielsen correction).

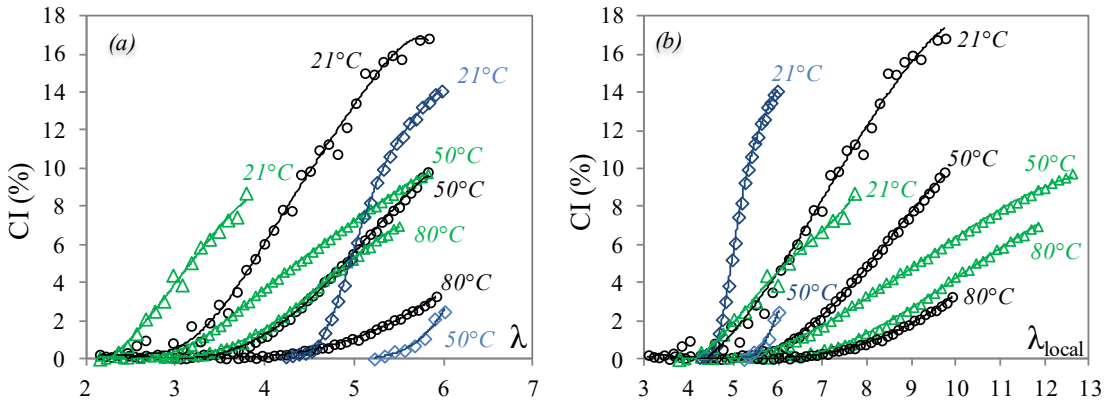

Figure 5. CI versus λ (a) or λ_{local} (b) during stretching at slow strain rate (4.2×10^{-3} s^{-1}) and various temperatures for NR (diamond symbols), F_{20}NR (circle symbols) and F_{50}NR (triangle symbols).

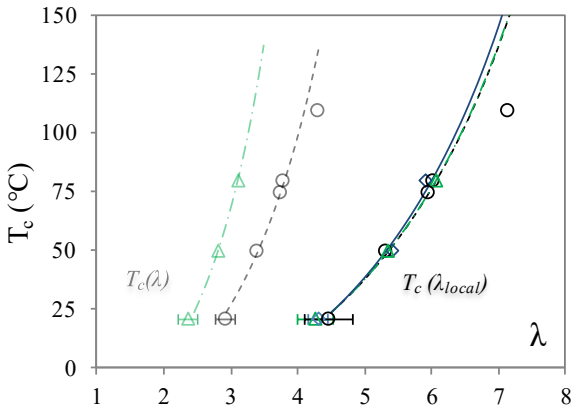

Figure 6. T_c versus λ and λ_{local} for NR (diamond symbols), F_{20}NR (circle symbols), F_{50}NR (triangle symbols). Prediction of T_c from equation (5) for NR (solid line), F_{20}NR (dotted

line) and $F_{50}NR$ sample (dashed-dotted line). The error bar is equal to +/-0.15 for λ_c at 21°C and +/-0.15*A* for $\lambda_{c,local}$ at 21°C (with *A* the amplification factor from the Nielsen correction).

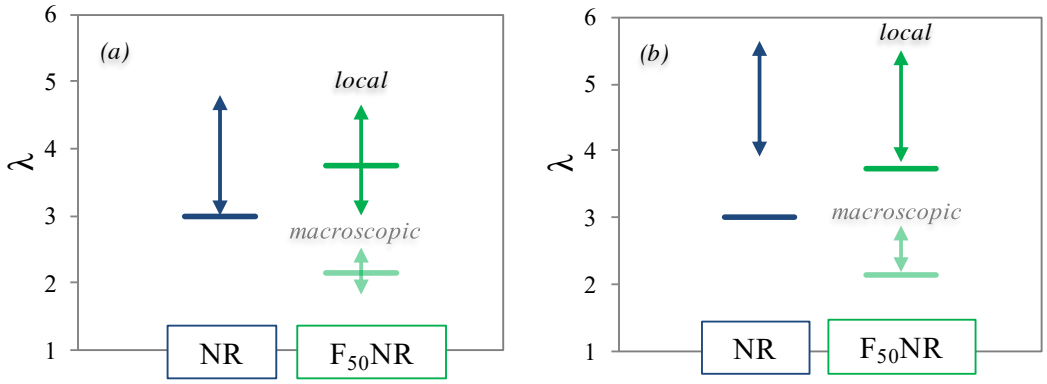

Figure 7. Dynamic tests performed with $\lambda_{min} \leq \lambda_m$ at 21°C (a) and with $\lambda_{min} > \lambda_m$ at 21°C (b). Arrows indicate the dynamic local and macroscopic amplitudes. Horizontal lines represent the λ_m and $\lambda_{m,local}$ values at 21°C.

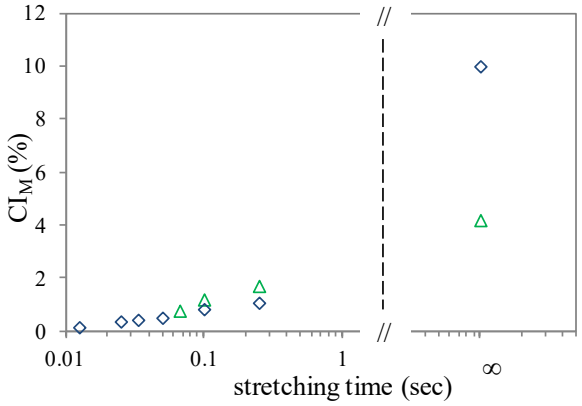

Figure 8. CI at λ_{max} (CI_M) versus stretching time for the first series of experiments and for NR (diamond) and F_{50}NR samples (triangle). CI at λ_{max} (CI_M) during the unloading phase of the cycles at slow strain rate are added (equilibrium state).

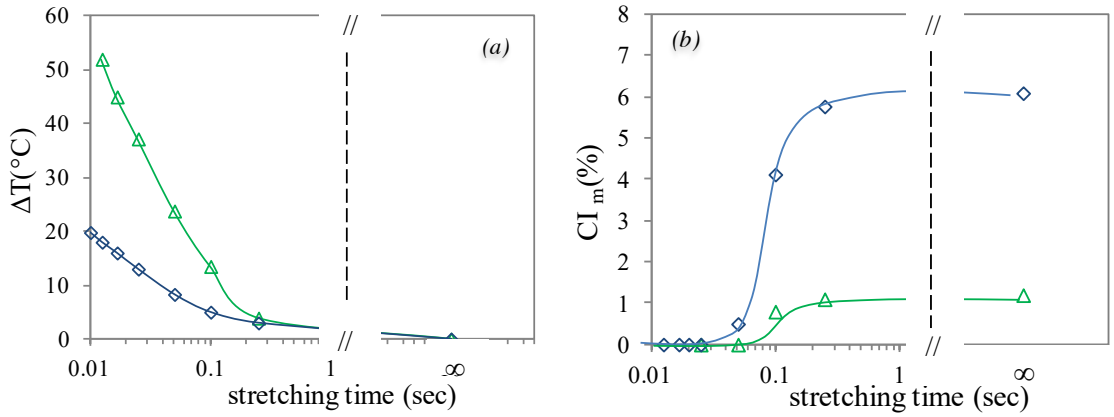

Figure 9. (a) Self-heating and (b) CI value at λ_{min} (CI_m) of NR sample (diamond symbols) and F_{50}NR sample (triangle symbols) versus stretching time for the second series of experiments. On figure 9b, the CI_m values measured during the unloading of the cycle at slow strain rate are added.

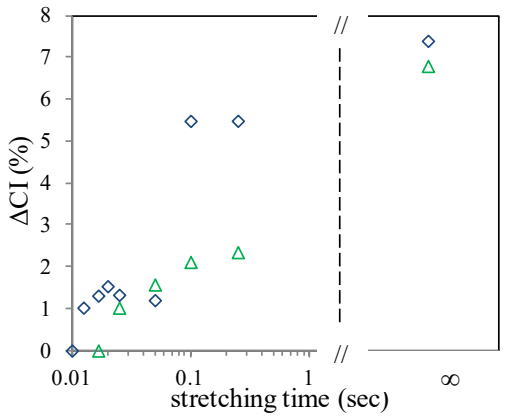

Figure 10. CI variation between λ_{min} and λ_{max} (ΔCI) versus the stretching time for the second series of experiments and for NR (diamond) and F_{50}NR samples (triangle). ΔCI measured during the unloading of the cycle at slow strain rate is added.

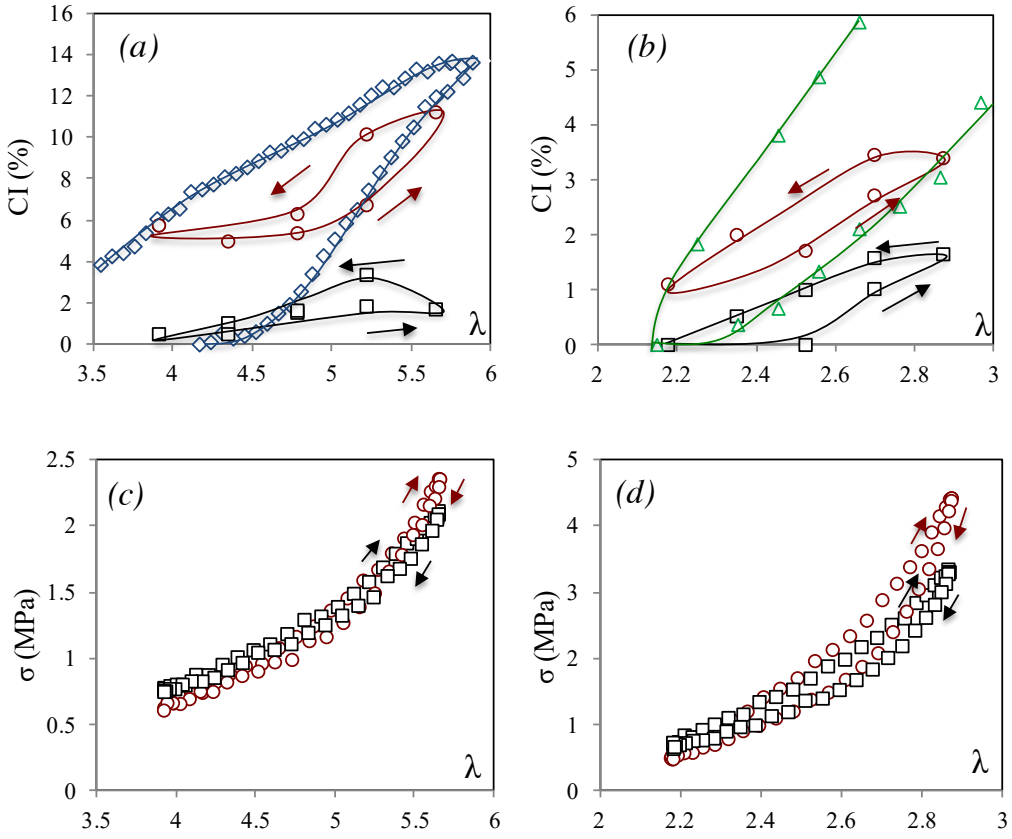

Figure 11. CI versus λ during dynamic tests of NR (a) and F_{50}NR (b) at 2 Hz (circles) and 10 Hz (squares). CI versus λ during slow strain rate cycle is added. Stress-strain curves for NR (c) and F_{50}NR (d).